Journal of Medicinal Chemistry

ARTICLE

pubs.acs.org/jmc

Discovery of 6-(2,4-Difluorophenoxy)-2-[3-hydroxy-1-(2-hydroxyethyl)propylamino]-8-methyl-8*H*-pyrido[2,3-*d*]pyrimidin-7-one (Pamapimod) and 6-(2,4-Difluorophenoxy)-8-methyl-2-(tetrahydro-2*H*-pyran-4-ylamino)pyrido[2,3-*d*]pyrimidin-7(8*H*)-one (R1487) as Orally Bioavailable and Highly Selective Inhibitors of p38α Mitogen-Activated Protein Kinase†

David M. Goldstein,* Michael Soth,* Tobias Gabriel, Nolan Dewdney, Andreas Kuglstatter, Humberto Arzeno, Jeffrey Chen, William Bingenheimer, Stacie A. Dalrymple, James Dunn, Robert Farrell, Sandra Frauchiger, JoAnn La Fargue, Manjiri Ghate, Bradford Graves,‡ Ronald J. Hill, Fujun Li, Renee Litman, Brad Loe, Joel McIntosh, Daniel McWeeney, Eva Papp, Jaehyeon Park, Harlan F. Reese, Richard T. Roberts, David Rotstein, Bong San Pablo, Keshab Sarma, Martin Stahl,§ Man-Ling Sung, Rebecca T. Suttman, Eric B. Sjogren, Yunchou Tan, Alejandra Trejo, Mary Welch, Paul Weller, Brian R. Wong, and Hasim Zecic

Roche Palo Alto LLC, 3431 Hillview Avenue, Palo Alto, California 94304, United States

Supporting Information

ABSTRACT: The development of a new series of p38α inhibitors resulted in the identification of two clinical candidates, one of which was advanced into a phase 2 clinical study for rheumatoid arthritis. The original lead, an lck inhibitor that also potently inhibited p38α, was a screening hit from our kinase inhibitor library. This manuscript describes the optimization of the lead to p38-selective examples with good pharmacokinetic properties.

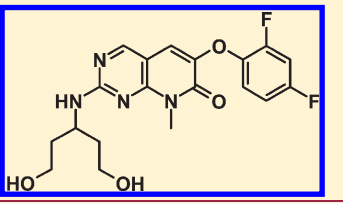

INTRODUCTION

p38 mitogen activated protein (MAP) kinases form a subfamily of the well-characterized MAP kinase family of serine/threonine kinases. p38 MAP kinases are widely expressed in endothelial, immune, and inflammatory cells and play a central role in regulating the production of cytokines including TNF-α, IL-1β, and IL-6.[1,2] Biologic agents targeting these cytokines or their receptors have proven efficacious for inflammatory diseases including rheumatoid arthritis (RA), psoriasis, and inflammatory bowel disease (IBD).[3,4]

The p38 subfamily of MAP kinases includes four isoforms (α, β, γ, and δ) that are encoded by separate genes. Recent analysis of synovial tissue extracted from RA patients suggests that the α and γ isoforms are overproduced within inflamed tissue and may be the preferred targets for intervention in the disease.[5−7] Several excellent reviews describing the potential importance of p38α MAP kinase (p38α) inhibitors as novel therapeutics for inflammatory diseases have been published.[8−11]

We previously reported the design and synthesis of 4-azaindole[12] and aminopyrazole[13] based p38α inhibitors. In this report, we describe our effort to optimize a lead compound identified through screening of our kinase inhibitor library as another piece of our overall strategy to advance multiple p38α inhibitors with novel scaffolds.

Lead compound **1**[14](Chart 1) was initially designed to be an inhibitor of lymphocyte specific protein tyrosine kinase (lck), a member of the src kinase family. The lead was very potent against lck but also showed significant potency against p38α (lck K_d = 0.2 nM, p38α K_d = 10 nM). Crystal structures of the lead bound to each enzyme showed that, while the molecule binds similarly to p38α and lck, there are important differences between the two inhibitor complexes. This paper highlights our successful efforts to engineer specificity toward p38α, which ultimately identified **2a** (R1487, Chart 1)[15] and **2b** (pamapimod, Chart 1)[16] as highly selective and orally bioavailable p38α inhibitors that were advanced into human clinical studies.[17−19]

RESULTS AND DISCUSSION

Chemistry. Two general routes were adopted for the syntheses of pyrimidinopyridones containing varied 2-, 6- and 8-substitution; representative syntheses are shown in Schemes 1 and 2. In the first route (Scheme 1), ethyl 4-chloro-2-methylthiopyrimidine-5-carboxylate was reacted with various amines to afford intermediate esters **3**, which were subsequently reduced to

Received: November 4, 2010
Published: March 04, 2011

Chart 1

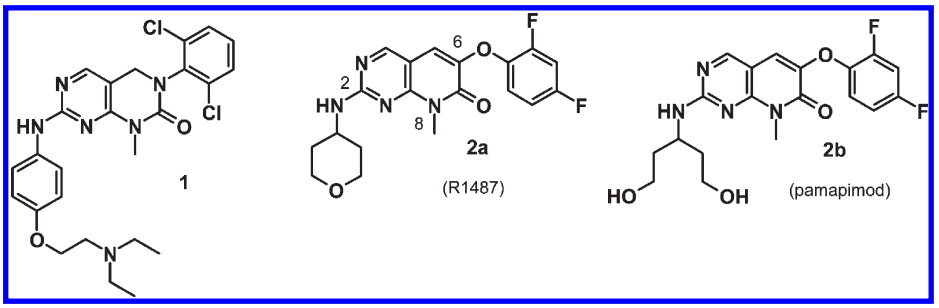

Scheme 1. Synthesis of Pyrimidinopyridones[a]

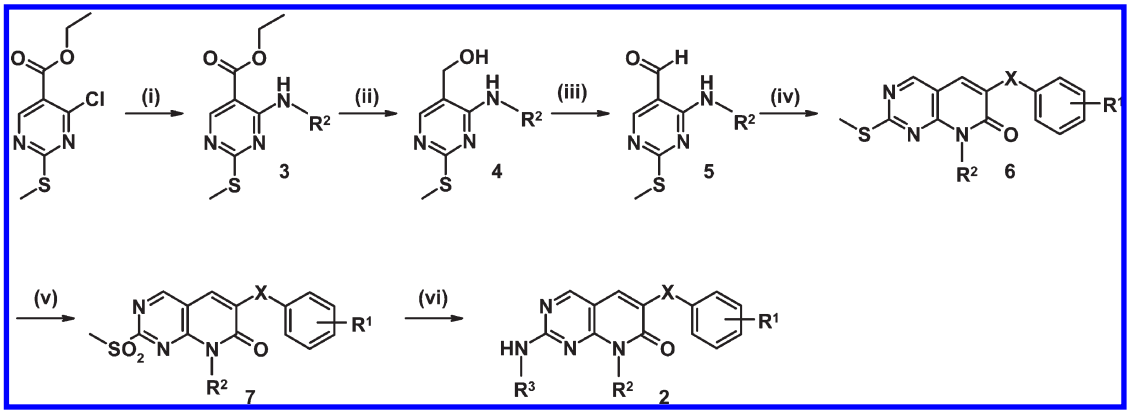

[a] Reagents and conditions: (i) R^2NH_2, 55−100%; (ii) $LiAlH_4$, 84−98%; (iii) MnO_2, 68−99%; (iv) $ArXCH_2CO_2Et$, base, 22−99%; (v) *m*CPBA or Oxone, 30−100%; (vi) R^3NH_2, base, 23−100%. **5a** (R^2 = Me) was a common intermediate for the preparations of **2a**−**j** and **2v**−**ii**. **7a** (R^2 = Me, XAr = 2,4-difluorophenoxy) was a common intermediate for the preparations of **2a**,**b** and **2v**−**ii**. In some cases, final products **2** were obtained as HCl salts. X = O, S, CH_2. For X = S, step v was omitted.

Scheme 2. Alternative Synthesis of Pyrimidinopyridones[a]

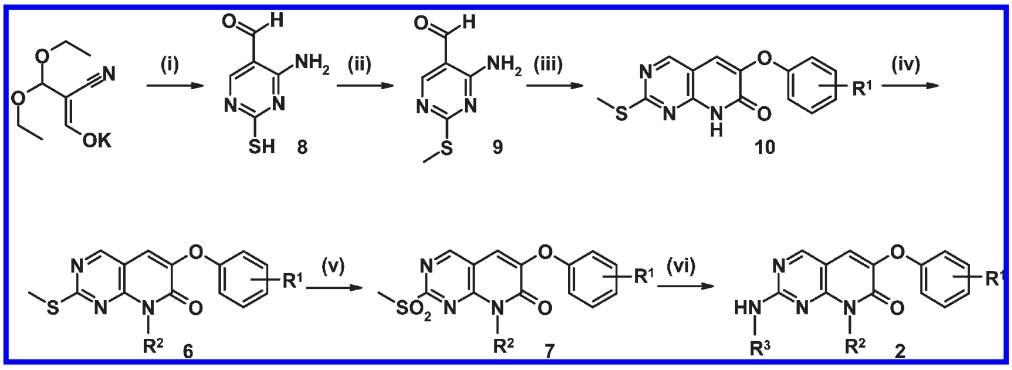

[a] Reagents and conditions: (i) thiourea, NaOMe, MeOH/EtOH, Δ, 72%; (ii) MeI, K_2CO_3, acetone, 95%; (iii) $EtOCOCH_2OAr$, K_2CO_3, NMP, 120 °C, 50%; (iv) R^2X, base or DEAD, R^2OH, PBu_3, 40−100%; (v) *m*CPBA or Oxone, 63−100%; (vi) R^3NH_2, base, 49−67%. In some cases, final products **2** were obtained as HCl salts. For **2k** (R^2 = H), step iv was omitted. **10a** (R^1 = 2,4-difluoro) was a common intermediate for the preparations of **2k**, **2o**, **2p**, **2r**, **2s**, and **2t**.

alcohols **4** and then oxidized to 4-aminopyrimidine-5-carboxaldehydes **5**. Aldehydes **5** were condensed with appropriately substituted acetates to afford the core pyrimidinopyridones **6**. The methylthio groups of pyrimidinopyridones **6** were oxidized to the corresponding sulfones **7**, which were displaced with amines to afford desired compounds **2**. This route was the most general and was required for 8-substituents more complex than straight chains.

The second route was used for some straight-chain 8-substituents and for the 8-unsubstituted analogue (Scheme 2). 2-Hydroxymethylene-3,3-diethoxypropionitrile potassium salt was condensed with thiourea to afford pyrimidinethiol **8**, which

dx.doi.org/10.1021/jm101423y |*J. Med. Chem.* 2011, 54, 2255–2265

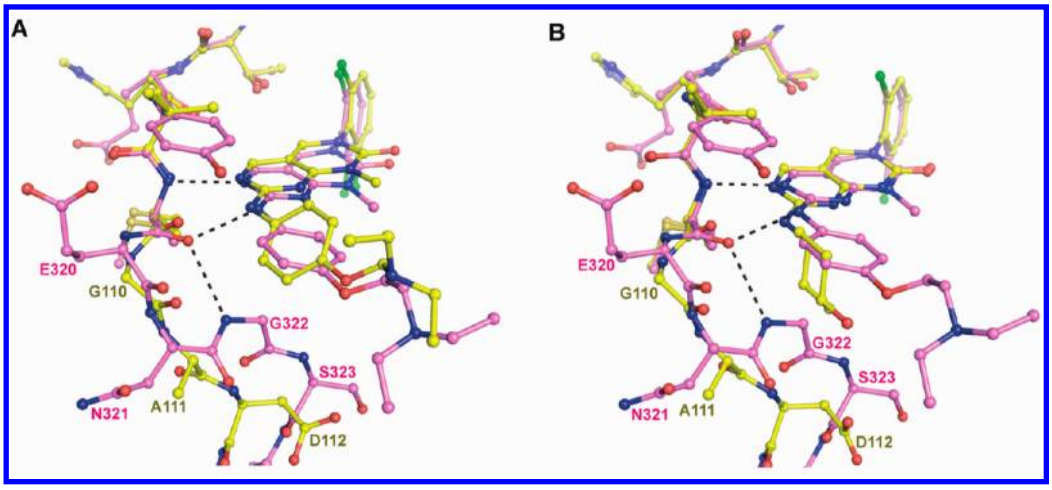

Figure 1. X-ray crystal structure of the lck−**1** complex (pink, 2.8 Å resolution, PDB accession code 3KMM) superimposed with structures of p38α (yellow) in complex with compound **1** (A, 2.1 Å, 3FSF) and compound **11** (B, 2.0 Å, 3FSK).

was reacted with methyl iodide to afford intermediate **9**. Compound **9** was condensed with ethyl 2,4-difluorophenoxyacetate to afford the core pyrimidinopyridone **10**, which could be alkylated at the 8-position with primary or isopropylalkyl halides (attempted reactions of pyrimidinopyridones **10** with more complex secondary halides or alcohols under Mitsunobu conditions led to O-alkylation). The final steps of the sequence were analogous to the first route.

Many varied syntheses were required for individual side chains and are detailed in the Experimental Section and Supporting Information.

Optimization of Kinase Selectivity. Our chemistry approach began with compound **1**, a lead identified from within the Roche kinase library. Compound **1** was initially designed to inhibit lck (lck K_d = 0.2 nM, p38α K_d = 10 nM). While lck shares relatively low sequence homology with p38α in the active site (41%), both enzymes contain threonine as the gatekeeper residue (Thr106 in p38α, Thr316 in lck) in the ATP binding pocket, which allows access to similarly sized hydrophobic binding domains. X-ray crystal structures of compound **1** bound to each kinase confirmed similar binding motifs in the active sites of both enzymes (Figure 1A).

The overlay of the two cocrystal structures revealed an opportunity to alter the kinase selectivity profile in favor of p38α over lck by taking advantage of the larger pocket in the lower lip portion of p38α (amino acids 111−113). The lower lip portion of p38α is larger than that of lck (amino acids 321−324) as a consequence of p38α lacking a residue corresponding to Gly322 in lck (Figure 1). This glycine residue, which is present in 345 human kinases, adopts a conformation favorable to an intramolecular hydrogen bond with the hinge portion of the protein (amino acids 317−320 in lck, amino acids 107−110 in p38α), reducing the overall size of the binding pocket.

Exchange of the aniline moiety of compound **1** with a saturated alkylamine increased the three-dimensional bulk of the molecule and caused unfavorable steric interactions between the inhibitor and the lower lip portion of lck kinase. This is exemplified by the structure of p38α complexed with compound **11**[20] (Chart 2, Figure 1B). Compound **11** showed dramatically improved selectivity for p38α over lck (p38α K_d = 32 nM, lck K_d > 20 μM).

In addition to this modification, the central pyrimidino*pyrimidone* core was converted to a pyrimidino*pyridone*, as it was

Chart 2

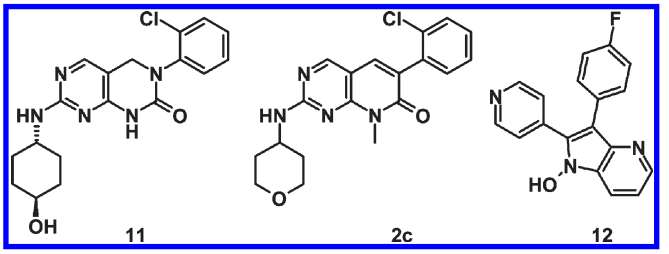

found that pyrimidinopyridones were generally more potent for p38α. The sum of these changes, exemplified by compound **2c**, effectively inverted a potent tyrosine kinase inhibitor class into one with improved selectivity versus the lck family tyrosine kinases and increased intrinsic potency for p38α (p38α K_d = 0.3 nM, lck K_d = 1800 nM). However, while these modifications did improve selectivity, kinase selectivity profiling of compound **2c** indicated that this compound still hits a large number of kinases (Figure 2). Pan-kinase selectivity was a general problem for this class of compounds. Compound **2c** was further profiled in a 14-day toxicity study and showed toxicity in spleen and kidney, as well as infections. We assumed that much of the toxicity was likely due to off-target kinase effects.

To further improve selectivity for p38α over other kinases, we turned to optimal space-filling of the backpocket. The size of the backpocket of kinases is defined by the gatekeeper residue, which in p38α is Thr106 (Figure 3A). The gatekeeper is a larger residue in many other kinases, thus offering the opportunity to design selectivity for p38α by optimal filling of this backpocket. Examination of the p38α-bound crystal structure of our previously disclosed azaindole inhibitor **12** (Chart 2),[12] which does effectively fill the backpocket (Figure 3B), inspired a simple modification of our newer series.

A comparison of the crystal structures for 6-phenylpyridone **2c** and azaindole **12** clearly shows that the directly linked phenyl side chain of **2c** is not filling the same hydrophobic volume as the phenyl side chain of **12** (Figure 3A,B). 6-Phenoxypyridones **2a** and **2d** were subsequently designed to position the phenoxy ring in the same space as the phenyl ring of **12**. X-ray crystallography confirmed that the binding motif enabled the phenoxy

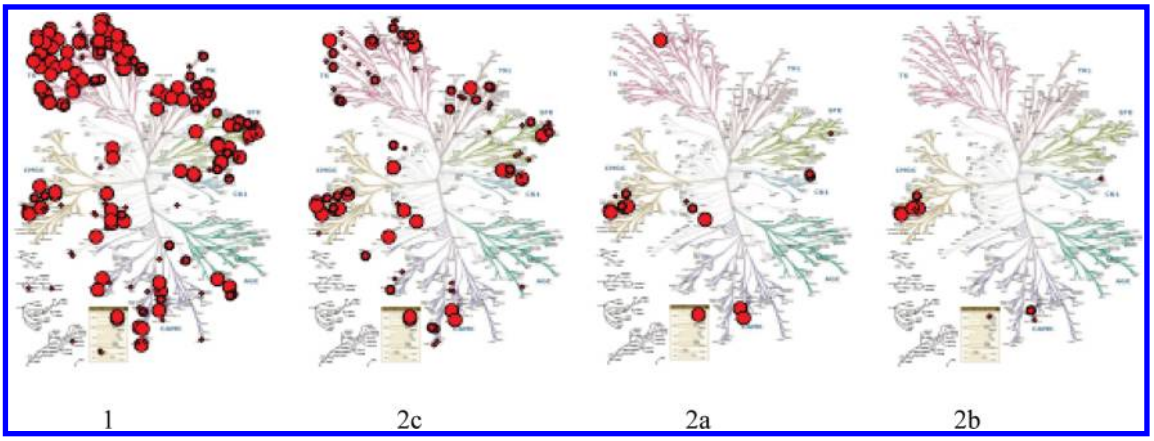

Figure 2. Evolution of the series with respect to kinase selectivity. The kinase dendrograms represent % ligand displacement at 10 μM test compound using the Ambit Biosciences kinase screen of >300 kinases; each branch corresponds to a different kinase. Large size dots represent 99−100% displacement. Medium size dots represent 91−99% displacement, and small size dots represent 51−91% displacement.

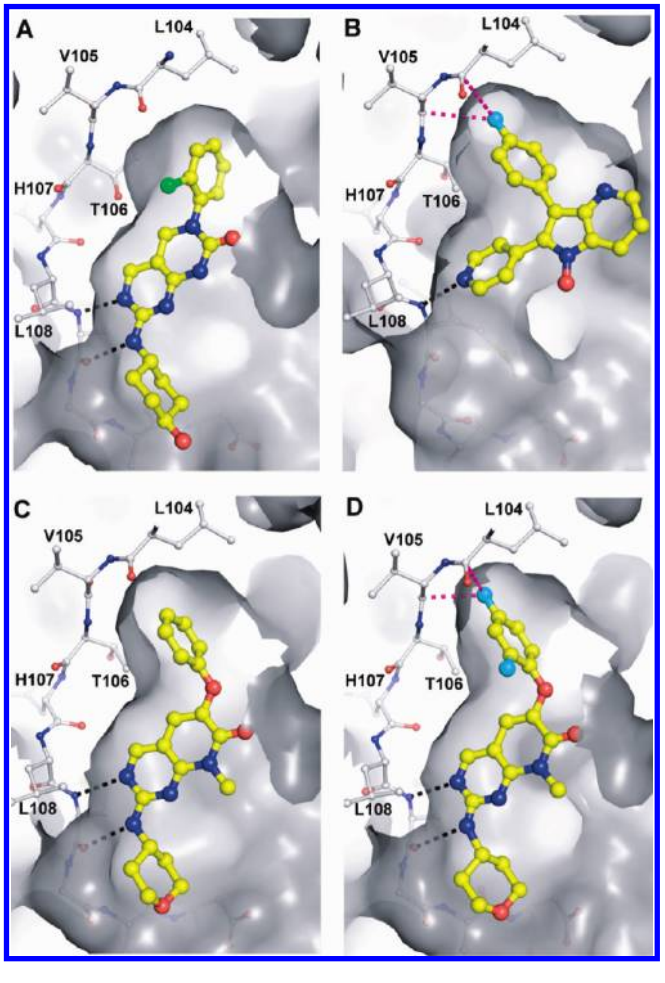

Figure 3. X-ray crystal structures of p38α in complex with (A) compound **11**, 2.0 Å resolution, PDB accession number 3FSK, (B) compound **12**, 2.1 Å, 1OZ1, (C) compound **2d**, 2.25 Å, 3FLZ, and (D) **2a**, 1.9 Å, 3FLN.

substituent to optimally fill the hydrophobic pocket accessible in p38α (Figure 3C,D). An alternative rotamer of the "gatekeeper" Thr106 relative to that observed in enzyme bound to **2c** deepens this pocket to accommodate the phenoxy group. Interestingly, the *p*-fluoro atom on the phenoxy moiety of **2a** is within 3.2 and 3.1 Å of the peptide carbonyl carbons of L104 and V105, respectively. This short distance may indicate a weak attractive interaction, the like of which has been described and carefully analyzed previously.[21,22] Comparison of the in vitro enzyme IC_{50} of the nonfluorinated analogue **2d** with the IC_{50} of 4-flouro compound **2e** (binding mode shown in Figure 3C) shows that the 4-fluorine increases ligand potency about 8-fold (Table 2). However, a similar comparison of the 2,4-difluoro example **2a** to the 2-fluoro analogue **2g** does not show the same boost in potency, suggesting that multiple factors influence the SAR for this side chain.

Most importantly, the kinase selectivity of 6-phenoxypyridone **2a** is greatly improved relative to the 6-phenylpyridones. After initial screening of the compounds at 10 μM versus >300 kinases,[23] the kinases inhibited were followed up with K_d determinations (10-point curve) for confirmation of inhibition and refinement of the selectivity profile. In the case of compound **2a**, detailed K_d determinations on the kinases inhibited in the single point screen confirmed submicromolar inhibition for only 10 out of >300 kinases tested (Figure 2, Table 1). High selectivity for p38α over other kinases is general for this series (2-alkylamino-6-phenoxypyrimidinopyridones), and this generality allowed us much freedom to explore substituents for optimal potency and druglike properties. Figure 2 also contains the kinase selectivity profile for our ultimate phase 2 candidate, **2b**, which shows submicromolar K_d for only seven out of >300 kinases tested (Figure 2, Table 1). Both compounds **2a** and **2b** bind to p38α and p38β isoforms but do not generally bind to either the p38γ or p38δ isoforms. Selectivity profiles for other key examples are similar.

SAR Studies. Tables 2−4 summarize the potency SAR for substitution at the 6-, 8-, and 2-positions of our pyrimidinopyridones. For most compounds, shifts in potency between our enzyme assay and our HWB (human whole blood) assay were relatively small (2- to 20-fold). Trends in SAR generally tracked between the two assays.

As discussed earlier in the manuscript, pan-kinase selectivity for our inhibitors is strongly dependent on the 6-substituent. This position is also sensitive with respect to potency (Table 2). 6-Aryl substituents such as the *o*-chlorophenyl of compound **2c** generally confer good potency (although poor pan-kinase selectivity). Many 6-phenoxy analogues (examples **2a**, **2d**−**g**)

Table 1. Kinase Selectivity of 2a and 2b[a]

	kinase assay K_d (nM)	
kinase	**2a**[b]	**2b**[c]
P38α	0.2	1.3
P38β	29	120
ADCK3	320	>1000
CSNK1ε	>1000	260
DDR1	270	>1,000
GAK	680	>1,000
JNK1	29	190
JNK2	9	16
JNK3	3	19
NLK	6	170
RSK2	150	300
RSK4	73	150
STK36	330	>1,000

[a] K_d values were determined for all kinases that demonstrated greater than 85% inhibition at 10 μM. [b] Versus 317 kinases (290 wild type). [c] Versus 353 kinases (321 wild type).

Table 2. Effect of Substitution at the 6-Position

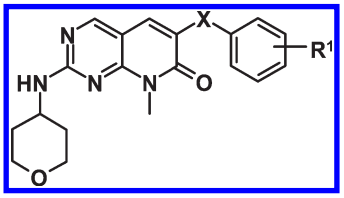

			assay IC_{50} (nM)[a]	
compd	X	R^1	p38α inhibition	HWB[b]
2a	O	2′,4′-diF	10 ± 4	200 ± 87
2c	bond	2′-Cl	21 ± 10	85.7 ± 43
2d	O	H	106 ± 36	451 ± 215
2e	O	4′-F	14 ± 6	547 ± 269
2f	O	3′-F	594 ± 211	1219 ± 597
2g	O	2′-F	15 ± 6	64.8 ± 28
2h	S	2′-F	111 ± 35	731 ± 261
2i	CH_2	2′-F	42 ± 15	407 ± 166
2j	CH_2	2′,4′-diF	40 ± 11	713 ± 242

[a] Mean ± SEM (standard error of the mean), $n \geq 3$. [b] Inhibition of TNF-α induced production of IL-1β.

have high potency (and good pan-kinase selectivity). 6-Phenylthio and 6-benzyl analogues are typically less potent than 6-phenoxy analogues (compare **2h** and **2i** to **2g**), and the corresponding 6-sulfones are inactive (data not shown).

We chose to focus on phenoxy substituents, since they gave rise to good potencies and promising kinase selectivity profiles. Further SAR on the phenoxy group revealed a preference for small ortho and para substituents over no substituents or meta-substitution. *o,p*-Difluoro substitution also optimized metabolic stability of this side chain (data not shown).

Table 3. Effect of Substitution at the 8-Position

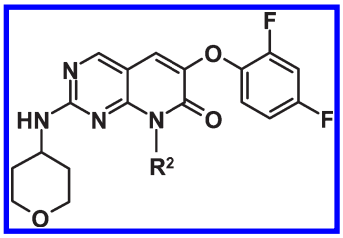

		assay IC_{50} (nM)[a]	
compd	R^2	p38α inhibition	HWB[b]
2a	Me	10 ± 4	200 ± 87
2k	H	18 ± 3	84 ± 80
2l	Et	1 ± 0.1	15 ± 7
2m	cyclopropyl	9 ± 1	13 ± 13
2n	$(CH_2)_3OH$	2 ± 0.5	14 ± 3
2o	$(CH_2)_2SO_2CH_3$	20 ± 4	308 ± 262
2p	$(CH_2)_3SO_2CH_3$	6 ± 0.5	18 ± 7
2q	1,1-dioxotetrahydro-2*H*-thiopyran	1 ± 0.2	11 ± 8
2r	$CH_2C(OH)(CH_3)_2$	12 ± 2	84 ± 66
2s	(*S*)-$CH_2CHOHCH_2OH$	7 ± 1	15 ± 9
2t	CH_2CN	2 ± 0.3	28 ± 19
2u	1-methanesulfonylpiperidinyl	1 ± 0.1	52 ± 23

[a] Mean ± SEM, $n \geq 3$. [b] Inhibition of TNF-α induced production of IL-1β.

Many different side chains are tolerated at the 8-position of the scaffold (Table 3), highlighting the fact that this vector points toward solvent (Figures 3 and 4). The SAR around this position was relatively flat. While other side chains did increase in vitro potencies, none offered any clear advantages over the original methyl group when considering metabolic stabilities and in vivo exposures (data not shown).

As described earlier in the manuscript, 2-alkylamino side chains show greater kinase selectivity than 2-anilino side chains; beyond this general consideration, we had considerable room to operate off the 2-position (Table 4). X-ray crystal structures of p38α−ligand complexes revealed that the scaffold can shift to allow optimal fitting for 2-substituents of varying size and stereochemistry (Figure 4C−F). This accommodation of the protein for changes in scaffold positioning lent much flexibility to variation at the 2-position, which turned out to be the most profitable one to explore in optimizing the physical properties of the series. Many examples with excellent properties were discovered; we highlight five of them in the next section.

Profiling of 2a, 2b, 2cc, 2ee, and 2hh. These five analogues from Table 4 were chosen for further studies, based on encouraging activities and properties in an acute in vivo PD model (Table 5).

Compound **2cc**, containing a chiral sulfone side chain, had good HWB activity, reasonable solubility, and high permeability. Further in vivo profiling in a rat model of lipopolysaccharide (LPS) induced production of TNF-α showed that **2cc** inhibited cytokine production by 88% at a dose of 3 mg/kg. However, the in vitro and in vivo stability of this compound was very high. Compound **2cc** in vivo showed low clearance in both rat and monkey as well as long half-lives (~24 h in monkey). Worries

dx.doi.org/10.1021/jm101423y |J. Med. Chem. 2011, 54, 2255–2265

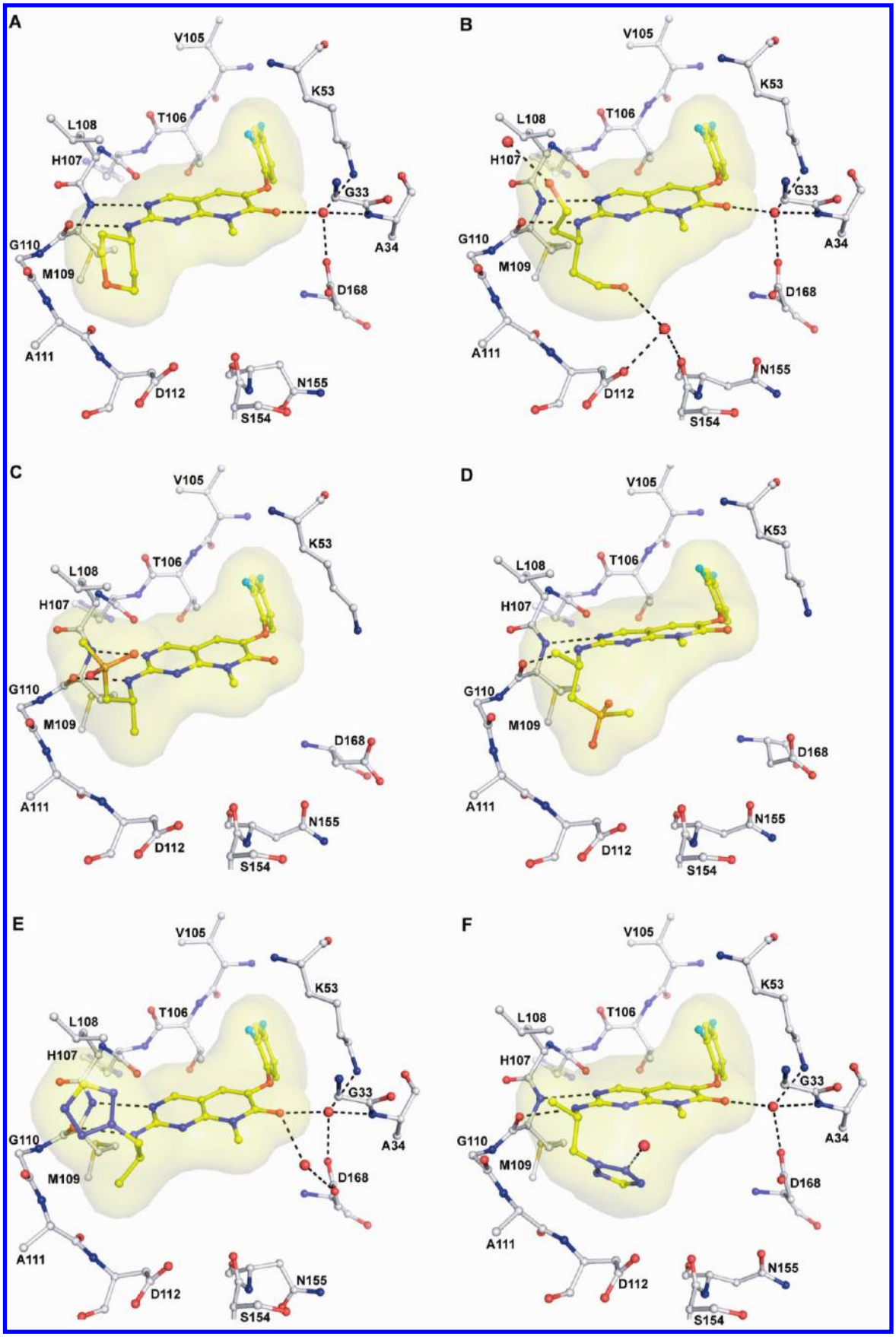

Figure 4. X-ray crystal structures of p38α in complex with (A) **2a**, 1.9 Å resolution, PDB accession number 3FLN, (B) **2b**, 2.1 Å, 3FLW, (C) **2cc**, 2.3 Å, 3FLS, (D) **2dd**, 1.9 Å, 3FLQ, (E) **2ii**, 1.9 Å, 3FMH, and (F) **2hh**, 1.7 Å, 3FMK.

dx.doi.org/10.1021/jm101423y |*J. Med. Chem.* 2011, 54, 2255–2265

over drug accumulation prompted a deprioritization of this compound.

Compound **2ee**, containing an achiral acetyl piperidine side chain, also performed well in all in vitro assays. This example had good in vivo PK profiles and demonstrated good inhibition of cytokine production in our rat LPS model (76% inhibition of TNF-α production at 3 mg/kg). The decision to deprioritize this compound was made based on a variety of toxicities observed preclinically in vivo.

Compound **2hh**, containing a novel chiral 2-tetrazole-containing side chain, was an exceptionally potent example in HWB and demonstrated reasonable solubility and permeability. Compound **2hh** also demonstrated good inhibition of cytokine production in our rat LPS model (90% inhibition of TNF-α production at 3 mg/kg). The overall profile for **2hh** was excellent; however, the compound was discovered significantly later than **2a** and **2b**. Therefore, compound **2hh** was held as a backup to **2a** and **2b**, which were already in the clinic.

From this series, **2a** was the first molecule identified that satisfied all of our selection criteria and was selected for advancement into GLP studies (in fact, this decision predated the discovery of many of the compounds described in this manuscript). Compound **2b** was later identified as a second clinical candidate.

Table 4. Effect of Substitution at the 2-Position

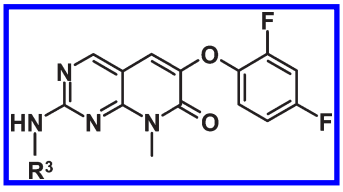

		assay IC_{50} (nM)[a]	
compd	R^3	p38α inhibition	HWB[b]
2a	4-tetrahydropyranyl	10 ± 4	200 ± 87
2b	$CH(CH_2CH_2OH)_2$	14 ± 2	100 ± 30
2v	Me	260 ± 75	
2w	isopropyl	4 ± 0.3	45 ± 30
2x	(*S*)-3-tetrahydrofuranyl	31 ± 8	373 ± 396
2y	$CH_2C(CH_3)_2OH$	67 ± 26	
2z	$C(CH_3)_2CH_2OH$	25 ± 8	
2aa	$CH(CH_2OH)_2$	158 ± 67	189 ± 94
2bb	$(CH_2)_2SO_2CH_3$	223 ± 74	1487 ± 771
2cc	(*R*)-$CHCH_3CH_2SO_2CH_3$	5 ± 1	50 ± 12
2dd	(*S*)-$CHCH_3CH_2SO_2CH_3$	50 ± 20	>3000
2ee	*N*-acetyl-4-piperidinyl	1 ± 0.6	30 ± 5
2ff	*trans*-4-hydroxycyclohexanyl	4 ± 0.6	68 ± 4
2gg	1,1-dioxotetrahydro-2*H*-thiopyran	15 ± 2	769 ± 309
2hh	(*S*)-$CHCH_3CH_2$(2-tetrazole)	2 ± 0.7	9 ± 1
2ii[c]	(*R*)-$CHCH_3CH_2$(2-tetrazole)	11	318

[a] Mean ± SEM, $n \geq 3$. [b] Inhibition of TNF-α induced production of IL-1β. [c] $n = 1$ data.

Pharmacological Evaluation of 2a and 2b[15]**.** The in vitro and in vivo pharmacology results for **2a** and **2b** are summarized in Table 6. Both compounds potently inhibited cytokine production in a variety of in vitro and in vivo models. Compounds **2a** and **2b** inhibited production of TNFα by human monocytic cells (THP-1) and inhibited production of IL-1β in human whole blood (HWB) induced by LPS.

In rodent models of acute inflammation, both **2a** and **2b** were dosed orally and evaluated for their ability to inhibit the production of TNFα and IL-6 after ip injection of LPS into Hanover Wistar rats. The compounds were administered to rats 0.5 h prior to challenge with 50 μg/kg LPS. Serum was collected 1.5 h after LPS injection for analysis of cytokines and concentrations of drug. **2a** and **2b** demonstrated significant dose-dependent inhibition of serum TNFα and IL-6. The estimated effective dose (ED) for TNFα inhibition is reported in Table 6.

In an alternative rat model, the compounds were administered to rats 0.5 h prior to challenge with TNFα. Serum was collected 2 h after ip injection of TNFα for analysis of cytokines and concentration of drug. The compounds inhibited TNFα-induced IL-6 at an ED_{50} ± ASE of 0.4−1.1 mg/kg. The plasma concentrations of the p38 inhibitors associated with efficacy in these acute rat in vivo cytokine assays were generally in close agreement to their in vitro IC_{50} in human cells.

Additionally, **2a** and **2b** were analgesic in vivo. In a rat model of inflammatory hyperalgesia, both compounds increased tolerance to pressure in a dose-dependent manner, suggesting that p38 inhibition may also reduce the pain associated with inflammation. The anti-inflammatory activities of **2b** in multiple cell, acute and chronic in vivo models of inflammation have been recently reported in greater detail.[18]

Pharmacokinetics and Metabolism of 2a. A summary of the pharmacokinetic parameters for **2a** is detailed in Table 7. Intravenous systemic clearance (Cl) of **2a** was variable across species: low in monkey, medium in rat, and very high in dog (exceeded hepatic blood flow). Volume of distribution at steady state (V_{dss}) was moderate in all species studies. Oral bioavailability of 10 mg/kg **2a** in monkey, rat, and dog was 51.6%, 29.3%, 10.3%, respectively. Absorption was fairly slow but mostly complete in rat and monkeys. Compound **2a** was moderately (90.4−95.6%) bound to rat, monkey, and dog plasma proteins

Table 5. Further Profiling of Most Promising Examples

parameter	2a	2b	2cc	2ee	2hh
aqueous solubility,[a] μg/mL	6	170	18	14	23
Caco2 permeability,[b] 10^6 cm/s	AB 33.0	AB 2.74	AB 13.5	AB 17.9	AB 30.1
	BA 23.7	BA 22.6	BA 22.4	BA 19.8	BA 19.7
human protein binding, % free	1.5	5.4	4.0	3.3	3.3
rat LPS 3 mg/kg, % inhibition	68	77	88	76	90

[a] Phosphate buffer, pH 6.5. [b] Permeability in Caco-2 cells AB (apical to basolateral) and BA (basolateral to apical) movement of 10 μM test compound in 21 day cultured Caco-2 cells ($(cm/s) \times 10^{-6}$), pH 7.4, on both sides.

dx.doi.org/10.1021/jm101423y |J. Med. Chem. 2011, 54, 2255–2265

Table 6. Summary of Biological Efficacy of 2a and 2b

	cell or animal model					
	in vitro IC_{50} (μM)		in vivo ED_{50} (mg/kg)/EC_{50} (μM) in rats[c]			
compd	THP-1[a] TNFα inhib	HWB[a] IL-1β inhib	LPS[b] TNFα inhib	LPS[b] IL-6 inhib	TNFα[b] IL-6 inhib	Yeast hyperalgesia
2a	0.047 ± 0.01	0.17 ± 0.02	(0.8 ± 0.29)/(0.03 ± 0.008)	(0.4 ± 0.07)/(0.01 ± 0.005)	(0.4 ± 0.17)/(0.02 ± 0.01)	5.5 ± 1.63
2b	0.025 ± 0.01	0.1 ± 0.03	(0.3 ± 0.07)/(0.12 ± 0.02)	(0.1 ± 0.03)/(0.05 ± 0.03)	(1.1 ± 0.33)/(0.27 ± 0.17)	(20.4 ± 4.8)/(4.3 ± 0.67)

[a] The data are expressed as the combined mean IC_{50} ± SEM. [b] The data are expressed as the combined mean ED_{50}/EC_{50} ± ASE (asymptotic standard error). [c] Data represent results from two independent rat experiments.

Table 7. Single Dose Plasma Pharmacokinetic Parameters of 2a after Dosing in Animals

	species, strain		
parameter	rat, Hanover-Wistar	monkey, Cynomolgus	dog, Beagle
dose (mg/kg)	10	10	10
gender	female	male	female
drug form	HCl salt	free base	HCl salt
sample size (iv, po)	60,[a] 3[b]	4, 3[b]	4, 3[b]
po T_{max} (h)	2.0	4.67	0.5
po C_{max} (μg/mL)	0.65	1.56	0.11
po $T_{1/2}$ (h)	ND	22.5	2.23
po AUC inf (μg·h/mL)	2.35	29.4	0.31
po *F* (%)	29.3	51.6	10.3
iv Cl ((L/h)/kg)	1.24	0.183	3.25
iv V_{dss} (L/kg)	1.94	2.73	4.65
% protein binding[c]	95.6	95.4	90.4

[a] The iv (intravenous) values are based on mean plasma concentrations; plasma from three rats per sample time. Formulation for iv dosing was aqueous 40% w/v cyclodextrin. [b] The po (per os) values are based on mean parameter; serial plasma samples obtained from each animal. Formulation for po dosing was aqueous 1% hydroxypropyl methylcellulose, 0.4% polysorbate 80, 0.9% benzyl alcohol, 0.04% citric acid monohydrate, 0.24% sodium citrate dihydrate. [c] The in vitro binding of [^{14}C]**2a** to plasma protein at 37 °C was studied by ultrafiltration methods.

Table 8. Single Dose Plasma Pharmacokinetic Parameters of 2b after Dosing in Fed Animals

	species, strain		
	rat, Hanover-Wistar	monkey, Cynomolgus	dog, Beagle
dose (mg/kg)	5	5	5
gender	female	male	female
sample size (iv, po)	56,[a] 56[b]	4, 3[b]	4, 3[b]
po T_{max} (h)	0.5	1.50	0.67
po C_{max} (μg/mL)	1.34	1.86	1.38
po $T_{1/2}$ (h)	4.04	13.8, est	9.18
po AUC (μg·h/mL) (0 to last *t*)	3.13, 24 h	9.41, 72 h	5.22
po *F* (%)	80.1	>100	78.2
iv Cl ((L/h)/kg)	1.26	0.65	0.75
iv V_{dss} (L/kg)	3.56	20.6	12.7
% protein binding[c]	82.9	85.4	ND

[a] The iv values are based on mean plasma concentrations; plasma from three rats per sample time. Formulation for iv dosing was aqueous 40% w/v cyclodextrin. [b] The po values are based on mean parameter; serial plasma samples obtained from each animal. Formulation for po dosing was aqueous 1% hydroxypropylmethylcellulose, 0.4% polysorbate 80, 0.9% benzyl alcohol, 0.04% citric acid monohydrate, 0.24% sodium citrate dihydrate. [c] The in vitro binding of [^{14}C]**2b** to plasma protein at 37 °C was studied by ultrafiltration methods.

and highly (98.5%, data not shown) bound to human plasma proteins. Rat and monkey plasma contained mostly **2a** but also metabolites including diol **2b**.

The human cytochrome P450 enzyme primarily responsible for the transformation of **2a** was 1A2. The IC_{50} values for inhibition of human cytochrome P450s, 1A2, 2C9, 2C19, 2D6, and 3A4 were all greater than 40 μM.

Pharmacokinetics and Metabolism of 2b. A summary of the pharmacokinetic parameters for **2b** is detailed in Table 8. Intravenous systemic clearance of **2b** was low to moderate across species Compound **2b** was well absorbed and had high oral bioavailability in the rat, monkey, and dog (62%−80%). Terminal elimination half-life ($T_{1/2}$) was moderate (~4 h) in rodents and high (>9 h) in monkeys and dogs. The elimination of **2b** was by metabolic clearance in the rat and by metabolic and renal clearance in the monkey. Compound **2b** was weakly (82.9% and 85.4%, respectively) bound to rat and monkey plasma proteins and moderately bound (94.6%, data not shown) to human plasma proteins.

Compound **2b** is neither a substrate nor a strong inhibitor of CYP450 enzymes (IC_{50} > 29 μM).

CONCLUSION

Our chemistry approach began with a molecule identified from within the Roche kinase library. A compound that was initially designed to inhibit lck was later demonstrated to inhibit p38α. An X-ray crystal structure of this lead compound confirmed similar binding motifs in the active sites of both enzymes and revealed opportunities to alter the kinase selectivity profile in favor of p38α. Incorporation of saturated alkylamines at the 2-position increased the three-dimensional bulk of the molecule and caused unfavorable steric interactions between the inhibitor and kinases containing a glycine insertion in the lower lip region. To further enhance the kinase selectivity profile, an additional template modification was made to expand the volume of the back hydrophobic pocket of p38α filled by the inhibitor series by insertion of an oxygen atom between the core scaffold and the aromatic ring. Indeed, an alternative rotamer of the "gatekeeper"

Thr106 deepens this pocket to accommodate the phenoxy group. To our satisfaction, in vitro studies demonstrated that optimized inhibitors **2a** and **2b** were highly potent and highly selective inhibitors of p38α. Further profiling of these inhibitors in a range of human cell assays, in vivo PK/PD and in vivo efficacy studies, pharmacokinetic parameters across multiple species, and safety studies supported the selection criteria for advancement of both **2a** and **2b** into human clinical trials. Compound **2b** was ultimately selected for advancement into phase 2 studies over **2a** based primarily on its superior pharmacokinetic profile in humans.

EXPERIMENTAL SECTION

Chemistry. Reagents and solvents were obtained from commercial suppliers and were used without further purification. Flash chromatography was performed with Merck silica gel 60 (230−400 mesh), and reaction progress was determined by thin-layer chromatography (TLC) on silica gel plates. Visualization was done with UV light (254 nm) or iodine. Yields were based on purified compounds and were not optimized. ^{1}H NMR measurements were recorded at 300 MHz using a Bruker AMX 300 instrument in DMSO-d_6 or $CDCl_3$ with tetramethylsilane as the internal standard. Melting points recorded were uncorrected. Purity and characterization of compounds were established by a combination of elemental analyses and NMR analytical techniques, and the purity was >95% by NMR for final products **2a** and **2b**. Elemental analyses on final products **2a** and **2b** were within ±0.4% for C, H, N.

4-Methylamino-2-methylthiopyrimidine-5-carboxaldehyde (5a). Methylamine in ethanol (33%, 35 mL, 280 mmol) was slowly added to a solution of ethyl 4-chloro-2-methylthiopyrimidine-5-carboxylate (20 g, 86 mmol) in 250 mL of dichloromethane at 0 °C. The solution was stirred for 30 min. Then 150 mL of water was added, and the layers were separated. The organic layer was dried over $MgSO_4$, filtered, and concentrated to 19 g (97%) of ethyl 4-methylamino-2-methylthiopyrimidine-5-carboxylate (**3a**) as a white solid. ^{1}H NMR (300 MHz, DMSO-d_6) δ ppm 1.30 (t, J = 7.25 Hz, 3 H), 2.49 (s, 3 H), 2.98 (d, J = 4.58 Hz, 3H), 4.28 (q, J = 7.25 Hz, 2 H), 8.19−8.28 (m, 1 H), 8.52 (s, 1 H).

A mixture of lithium aluminum hydride (8.2 g, 210 mmol) in 300 mL of dry tetrahydrofuran at 5 °C was treated dropwise with a solution of ethyl 4-methylamino-2-methylthiopyrimidine-5-carboxylate (46 g, 200 mmol) in 450 mL of dry tetrahydrofuran. The reaction mixture was stirred for 15 min, and then 18 mL of water was added dropwise with caution. The mixture was stirred for 30 min. Then 8.5 mL of a 15% aqueous NaOH solution was added dropwise, followed by 25.5 mL of water. The resulting suspension was stirred for 17 h at room temperature and then filtered. The filter residue was sequentially washed with two 100 mL portions of tetrahydrofuran, and the combined filtrate and washings were concentrated to a residue. The residue was suspended in 200 mL of a 2:1 ethyl acetate/hexane solution, and a yellow solid was isolated by filtration and dried to provide 32.7 g (88%) of 4-methylamino-2-methylthiopyrimidine-5-methanol (**4a**). ^{1}H NMR (300 MHz, DMSO-d_6) δ ppm 2.43 (s, 3 H) 2.86 (d, J = 4.58 Hz, 3 H), 4.31 (d, J = 5.34 Hz, 2 H), 5.10 (t, J = 5.34 Hz, 1 H), 6.82 (d, J = 4.58 Hz, 1 H), 7.82 (s, 1 H).

4-Methylamino-2-methylthiopyrimidine-5-methanol (20 g, 110 mmol) and 1 L of dichloromethane were combined with stirring and treated with manganese dioxide (87 g, 1.0 mol). The resulting suspension was stirred for 24 h and then filtered through Celite. The filter residue was washed with 100 mL of dichloromethane, and the combined filtrate and washings were concentrated to give 15.8 g (80%) of 4-methylamino-2-methylthiopyrimidine-5-carboxaldehyde as a white solid. Mp 101.7−102.3 °C . ^{1}H NMR (300 MHz, DMSO-d_6) δ ppm 2.51 (s, 3 H), 2.99 (d, J = 4.91 Hz, 3 H), 8.50 (s, 1 H), 8.63 (d, J = 3.78 Hz, 1 H), 9.74 (s, 1 H). MS (EI/CI) m/z: 184 (M + H).

6-(2,4-Difluorophenoxy)-2-methanesulfonyl-8-methyl-8*H*-pyrido[2,3-*d*]pyrimidin-7-one (7a). A mixture of 4-methylamino-2-methylthiopyrimidine-5-carboxaldehyde (**5a**) (4.8 g, 26 mmol) and methyl 2,4-difluorophenoxyacetate (5.4 g, 29 mmol) in 50 mL of 1-methyl-2-pyrrolidinone was treated with potassium carbonate (6.0 g, 44 mmol). The reaction mixture was stirred at 120 °C for 12 h. Additional methyl 2,4-difluorophenoxyacetate (2.5 g, 13 mmol) and potassium carbonate (2.5 g, 18 mmol) were added. The mixture was stirred at 120 °C for an additional 6 h, then cooled to room temperature. Water (100 mL) was added, and the solution was stirred for 45 min and then filtered. The resulting solid was washed three times with water, added to 75 mL of ethyl acetate, and the resulting mixture was stirred for 1 h. The solid was then isolated by filtration and dried to yield 6.1 g (69%) of 6-(2,4-difluorophenoxy)-8-methyl-2-methylsulfanyl-8*H*-pyrido[2,3-*d*]pyrimidin-7-one (**6a**). ^{1}H NMR (300 MHz, DMSO-d_6) δ ppm 2.59 (s, 3 H), 3.66 (s, 3 H), 7.05−7.20 (m, 1 H), 7.35 (td, J = 9.35, 5.72 Hz, 1 H), 7.41 (s, 1 H), 7.51 (ddd, J = 11.44, 8.77, 3.05 Hz, 1 H), 8.82 (s, 1 H).

A solution of 6-(2,4-difluorophenoxy)-8-methyl-2-methylsulfanyl-8*H*-pyrido[2,3-*d*]pyrimidin-7-one (50 g, 0.15 mol) in 420 mL of dichloromethane was treated with formic acid (17 g, 0.37 mol), followed by portionwise addition of a 30% aqueous hydrogen peroxide solution (71 g, 0.63 mol), then stirred at 38 °C until reaction completion as confirmed by area normalized HPLC. The resulting light yellow solution was cooled to <25 °C. Then 32 mL of water was added, and layers were separated. The organic layer was washed with an aqueous NaOH solution (5 g of NaOH in 53 mL of H_2O). Then dichloromethane was exchanged to 160 mL of *tert*-butyl methyl ether. The solution was cooled to <5 °C, and precipitate was isolated by filtration, washed with 36 mL of *tert*-butyl methyl ether, and dried on the filter to afford 38 g (71%) of 6-(2,4-difluorophenoxy)-2-methanesulfonyl-8-methyl-8*H*-pyrido[2,3-*d*]pyrimidin-7-one. Mp 182.2−183.0 °C. ^{1}H NMR (DMSO-d_6) δ 3.47 (s, 3 H), 3.74 (s, 3 H), 7.17−7.28 (m, 1 H), 7.40−7.52 (m, 2 H), 7.61 (ddd, J = 11.21, 8.76, 3.01 Hz, 1 H), 9.18 (s, 1 H). MS (EI/CI) m/z: 368 (M + H).

6-(2,4-Difluorophenoxy)-8-methyl-2-(tetrahydro-2*H*-pyran-4-ylamino)pyrido[2,3-*d*]pyrimidin-7(8*H*)-one (2a). A suspension of 6-(2,4-difluorophenoxy)-2-methanesulfonyl-8-methyl-8*H*-pyrido[2,3-*d*]pyrimidin-7-one (**7a**) (55 g, 150 mmol), sodium carbonate (16.5 g, 156 mmol), and 4-aminotetrahydropyran (22.00 g, 217.5 mmol) in 150 mL of toluene was stirred at 80 °C overnight. The reaction mixture was diluted with 500 mL of toluene, and the hot suspension was filtered. The filtrate was allowed to cool, and precipitated solid was isolated by filtration, washing with 100 mL of water and then 100 mL of a 1:1 methanol/water solution, to afford 53 g (90%) of 6-(2,4-difluorophenoxy)-8-methyl-2-(tetrahydro-2*H*-pyran-4-ylamino)pyrido-[2,3-*d*]pyrimidin-7(8*H*)-one. Mp 185.7−187.5 °C. ^{1}H NMR (DMSO-d_6) δ 1.56 (qd, J = 11.83, 4.20 Hz, 2 H), 1.87 (br s, 2 H), 3.41 (t, J = 10.68 Hz, 2 H), 3.49−3.64 (m, 3 H), 3.89 (d, J = 11.06 Hz, 2 H), 4.02 (br s, 1 H), 6.97−7.10 (m, 1 H), 7.18 (td, J = 9.16, 5.72 Hz, 1 H), 7.35−7.53 (m, 2 H), 7.57−7.85 (m, 1 H), 8.57 (s, 1 H). MS (EI/CI) m/z: 389 (M + H).

6-(2,4-Difluorophenoxy)-2-[3-hydroxy-1-(2-hydroxy-ethyl)-propylamino]-8-methyl-8*H*-pyrido[2,3-*d*]pyrimidin-7-one (2b). A 1.0 M solution of lithium aluminum hydride in tetrahydrofuran solution (571 mL, 571 mmol), under mechanical stirring at less than −10 °C, was slowly treated with 3-aminopentanedioic acid dimethyl ester (50.0 g, 285 mmol) in 50 mL of tetrahydrofuran, keeping the temperature under 20 °C. The reaction mixture was stirred at room temperature for 18 h, then cooled to less than −10 °C. Water (41 mL, 2.3 mol) was slowly added as the mixture was vigorously stirred, keeping the temperature under 20 °C. Diethylamine (33 mL, 320 mmol) was added to the mixture, which was then stirred at room temperature for 1 h. The solids were removed by

filtration and the filtrate was concentrated under vacuum at 45 °C to afford 13.7 g (40%) of 3-aminopentane-1,5-diol as an oil. ^{1}H NMR (CD_3OD) δ 3.67 (m, 4 H), 3.02 (tt, J = 8.11, 4.8 Hz, 1 H), 1.60 (m, 4 H).

Hexamethyldisilazane (20 mL, 96 mmol) and chlorotrimethylsilane (0.5 mL, 4 mmol) were added to 3-aminopentane-1,5-diol (9.6 g, 81 mmol) in 40 mL of tetrahydrofuran. The mixture was stirred at reflux for 18 h. Solvents were removed under vacuum at 45 °C, and the remaining oil was distilled under vacuum at 85−107 °C to afford 17.7 g (83%) of 3-trimethylsilanyloxy-1-(2-trimethylsilanyloxyethyl)propylamine as an oil. ^{1}H NMR ($CDCl_3$) δ 3.65 (m, 4 H), 2.97 (tt, J = 8.39, 4.3 Hz, 1 H), 1.51 (m, 6 H), 0.05 (s, 18 H).

A solution of 6-(2,4-difluorophenoxy)-2-methanesulfonyl-8-methyl-8*H*-pyrido[2,3-*d*]pyrimidin-7-one (**7a**) (10.0 g, 27.2 mmol), 3-trimethylsilanyloxy-1-(2-trimethylsilanyloxyethyl)propylamine (9.4 g, 36 mmol), and *N*,O-bis(trimethylsilyl)acetamide (3.55 mL, 14.4 mmol) in 20 mL of tetrahydrofuran was stirred at reflux overnight. The reaction mixture was concentrated under vacuum and the residue stirred in a mixture of 25 mL of *tert*-butyl methyl ether and an aqueous K_2HPO_4 solution (2 g in 50 mL of water). Precipitate was isolated by filtration and sequentially washed with water, 20 mL of a 30:70 methanol/water mixture, and 20 mL of toluene to afford 10.3 g (93%) of 6-(2,4-difluorophenoxy)-2-[3-hydroxy-1-(2-hydroxyethyl)propylamino]-8-methyl-8*H*-pyrido[2,3-*d*]pyrimidin-7-one. Mp 157.4−158.2 °C. ^{1}H NMR (DMSO-d_6) δ 1.62−1.86 (m, 4 H), 3.41−3.53 (m, 4 H), 3.53−3.65 (m, 3 H), 4.17−4.35 (m, 1 H), 4.40 (t, J = 5.05 Hz, 2 H), 7.03 (d, J = 7.07 Hz, 1 H), 7.10−7.25 (m, 1 H), 7.37−7.53 (m, 2 H), 7.59 (d, J = 8.59 Hz, 1 H), 8.50−8.61 (m, 1 H). MS (EI/CI) m/z: 407 (M + H).

Biological Methods. p38 MAP Kinase Inhibition. *HTS Assay.* HTS was performed using a Zymark robotic system and a 96-well, radioactive filtration binding format. The enzyme was preincubated with test compounds (40 μM) for 10 min at 30 °C, following which the reaction was initiated by adding [^{33}P]ATP (250 μM) and myelin basic protein (150 μM). Following an additional incubation for 20 min at 30 °C the reaction was terminated, and the radiolabeled product was captured on nitrocellulose filtration plate, washed, and counted for radioactivity. Compounds that displayed >40% inhibition of the enzyme activity were retested at multiple concentrations.

In Vitro Assay. Inhibition of human recombinant active p38α [5 nM] was tested by measuring the incorporation of ^{33}P from γ-[^{33}P]ATP [50 μM, 1 μCi] into myelin basic protein (MBP) [35 μM]. The assay was performed in a 96-well microtiter plate. In a 40 μL reaction volume, an amount of 26 μL of diluted p38α [5 nM] in assay dilution buffer (ADB) (20 mM MOPS, pH 7.4, 40 mM $MgCl_2$, 1 mM DTT, 25 mM β-glycerol phosphate, 5 mM EGTA, 1 mM sodium orthovanadate) was preincubated at room temperature for 10 min with 4 μL of test compounds [0−100 μM] dissolved in dimethylsulfoxide (DMSO) [10%]. The kinase reaction was initiated by the addition of 10 μL of assay mix, containing ADB and γ-[^{33}P]ATP [50 μM, 1 μCi] and MBP [35 μM]. After 30 min at 30 °C the reactions were stopped by the removal of 25 μL of reaction sample onto 200 μL of 0.75% phosphoric acid (H_3PO_4) containing acid prewetted Multiscreen 96-well phosphocellulose filter plate (Millipore). The plate membranes were washed three times with 200 μL of 0.75% H_3PO_4 for the removal of the free radionucleotide. Then 50 μL of Microscint-20 scintillant (Packard) was added to each well. The plate was sealed with a plastic film and counted in a Packard Topcount microplate scintillation counter. The 50% inhibitory value was calculated by fitting the data to the equation

$$\text{fractional activity} = \frac{1/[\text{I}]}{\text{IC}_{50} + 1}$$

Inhibition of TNF Biosynthesis. THP1 cells were suspended in culture medium [RPMI (Gibco-BRL, Gailthersburg, MD) containing 15% fetal bovine serum and 0.02 mM 2-mercaptoethanol, at 2.5 × 10^6 cells/mL, and then plated in a 96-well plate (0.2 mL aliquots in each well). Test compounds were dissolved in DMSO and then diluted with the culture medium such that the final DMSO concentration was 5%. Then 25 μL aliquots of test solution or medium with DMSO (control) were added to each well. The cells were incubated for 30 min at 37 °C. LPS (Sigma, St. Louis, MO) was added to the wells at a final concentration of 0.5 μg/mL, and cells were incubated for an additional 2 h. At the end of the incubation period, culture supernatants were collected and the amount of TNF-α present was determined by a specific trapping ELISA assay using two anti-TNF-α antibodies (2TNF-H22 and 2TNF-H34) as described.[16]

Inhibition of TNFα and IL-1β Biosynthesis in LPS-Stimulated Peripheral Blood Mononuclear Cells. Blood was collected from healthy volunteers (drug-free for 2 weeks) into vacutainers (Becton Dickinson, Mountainview, CA) containing 19 units/mL sodium heparin. Peripheral blood mononuclear cells (PBMC) were separated using a Histopaque-1077 gradient (Sigma, H-8889). Briefly, whole blood was diluted 1:1 in Dulbecco's phosphate-buffered saline (Gibco, no. 14190-136) and layered onto the histopaque solution followed by centrifugation at 400*g* for 20 min at room temperature. Cells were collected and washed once in cold PBS followed by red cell lysis with lysing media (Sigma no. R-7757, lot no. 46H2373). A final cell suspension was prepared at 2 × 10^6 per mL in RPMI 1640 (Gibco BRL, no. 11875-085), 10% FBS, 2 mM L-glutamine, and 5.5 × 10^{-5} M β-mercaptoethanol. Dilutions of test compounds were predispensed in 25 μL aliquots (before addition of cells) into round-bottom 96-well plates (U bottom TC plate; Costar no. 3799). The starting concentration was 100 μM in 5% DMSO, and six half log serial dilutions were made. After the addition of 200 μL of cell suspension and 25 μL of 5 μg/mL lipopolysaccharide (LPS, *E. coli*; 0127; B8; catalog no. L3129, Sigma Chem Co., St. Louis, MO) in medium, the final DMSO concentration was 0.5%. Aliquots of test compounds were diluted an additional 10-fold, and the final LPS concentration was 500 ng/mL. PBMC suspension (200 μL per sample) was preincubated with the diluted compound for 30 min at 37 °C followed by addition of 25 μL of LPS dissolved in RPMI (Gibco BRL, no. 11875-085) to produce a final LPS concentration of 0.5 μg/mL. Negative control wells received RPMI alone. Plates were incubated for 2 or 5 h at 37 °C in a 5% CO_2 atmosphere for determination of TNFα or IL-1β, respectively, followed by centrifugation at 150*g* for 10 min. Supernatants were collected from each sample and stored in polypropylene plates at 4 °C. TNF-α and IL-1β were determined by Elisa (Antibody Solutions, Palo Alto, CA) following the manufacturer's instructions. Optical density of each sample was read at 450 nm with a reference of 650 nm. Cytokine concentrations were determined from a standard curve using Molecular Devices SoftMax Pro. The percent inhibition was calculated for each concentration tested, and an IC_{50} curve was constructed using Xlfit software.

Phamacokinetics. Female Wistar/Han (CRL:WI) Rats (Charles River, Hollister, CA) weighing between 180 and 220 g were used. Beagle dogs (~5−10 kg) and cynomologous monkeys (5−8 kg) were residents of the facility animal colony. Animals were allowed free access to a standard laboratory chow and tap water and were housed in a constant temperature−humidity environment. All studies were conducted under IACUC approved protocols. Animals were administered either single iv bolus doses (50% cyclodextran/water) or single oral suspension doses prepared in aqueous vehicle containing 0.9% NaCl, 0.5% sodium carboxymethyl cellulose, 0.4% polysorbate 80, and 0.9% benzyl alcohol. Blood was collected from each animal with anesthesia at typically 0.08, 0.25, 0.5,1, 2, 3,4, 6, 8, and 24 h after dosing into tubes containing EDTA. Plasma concentrations of **6f** and/or **6x** were determined by a liquid chromatography/tandem mass spectrometry method (LC/MS/MS). **6f** or **6x** and an internal standard were extracted from samples by protein precipitation using acetonitrile. The supernatant was diluted using 0.1% formic acid and analyzed using liquid chromatography (LC) with tandem mass spectrometric detection (MS/MS). The standard curve

range for this assay is from 5.00 to 5000 ng/mL for **6f** and **6x** using a plasma sample volume of 0.100 mL.

Plasma Protein Binding. The in vitro binding of [^{14}C]**6x** to plasma protein at 37 °C was studied by ultrafiltration methods

Protein Crystallography. X-ray crystal structures of p38α−ligand complexes where determined following published procedures.[12] Atomic coordinates and structure factor amplitudes have been deposited to the RCSB PDB along with detailed statistics on data collection and structure refinement.

■ ASSOCIATED CONTENT

Supporting Information. Experimental procedures for intermediate **10a** and final compounds **2c**−**ii**. This material is available free of charge via the Internet at http://pubs.acs.org.

Accession Codes

[†]Structures are deposited in the RCSB Protein Data Bank under 3KMM, 3FLN, 3FLQ, 3FLS, 3FLW, 3FLZ, 3FMH, 3FMK, 3FSF and 3FSK.

■ AUTHOR INFORMATION

Corresponding Author

*For D.M.G.: phone, 973-235-4008; fax, 973-235-6263; e-mail, David-M.Goldstein@roche.com. For M.S.: phone, 973-235-2717; fax, 973-235-6263; e-mail, Michael.soth@roche.com.

Present Addresses

[‡]Hoffmann-La Roche Inc., Nutley, NJ.

[§]F. Hoffmann-La Roche Ltd., Basel, Switzerland.

■ ABBREVIATIONS USED

IBD, inflammatory bowel disease; lck, lymphocyte specific protein tyrosine kinase; LPS, lipopolysaccharide; MAP, mitogen activated protein; RA, rheumatoid arthritis; SAR, structure−activity relationship

■ REFERENCES

(1) Schett, G.; Zwerina, J.; Firestein, G. The p38 mitogen-activated protein kinase (MAPK) pathway in rheumatoid arthritis. *Ann. Rheum. Dis.* **2008**, *67*, 909–916.

(2) Westra, J.; Limburg, P. C. p38 mitogen-activated protein kinase (MAPK) in rheumatoid arthritis. *Mini-Rev. Med. Chem.* **2006**, *6*, 867–874.

(3) Schett, G.; Stach, C.; Zwerina, J.; Voll, R.; Manger, B. How antirheumatic drugs protect joints from damage in rheumatoid arthritis. *Arthritis Rheum.* **2008**, *58*, 2936–2948.

(4) Strand, V.; Singh, J. A. Improved health-related quality of life with effective disease-modifying antirheumatic drugs: evidence from randomized controlled trials. *Am. J. Manag. Care* **2008**, *14*, 234–254.

(5) Hale, K. K.; Trollinger, D.; Rihanek, M.; Manthey, C. L. Differential expression and activation of p38 mitogen-activated protein kinase alpha, beta, gamma, and delta in inflammatory cell lineages. *J. Immunol.* **1999**, *162*, 4246–4252.

(6) Korb, A.; Tohidast-Akrad, M.; Cetin, E.; Axmann, R.; Smolen, J.; Schett, G. Differential tissue expression and activation of p38 MAPK alpha, beta, gamma, and delta isoforms in rheumatoid arthritis. *Arthritis Rheum.* **2006**, *54*, 2745–2756.

(7) Schett, G.; Tohidast-Akrad, M.; Smolen, J. S.; Schmid, B. J.; Steiner, C. W.; Bitzan, P.; Zenz, P.; Redlich, K.; Xu, Q.; Steiner, G. Activation, differential localization, and regulation of the stress-activated protein kinases, extracellular signal-regulated kinase, c-JUN N-terminal kinase, and p38 mitogen-activated protein kinase, in synovial tissue and cells in rheumatoid arthritis. *Arthritis Rheum.* **2000**, *43*, 2501–2512.

(8) Goldstein, D. M.; Gabriel, T. Pathway to the clinic: inhibition of P38 MAP kinase. A review of ten chemotypes selected for development. *Curr. Top. Med. Chem.* **2005**, *5*, 1017–1029.

(9) Pettus, L. H.; Wurz, R. P. Small molecule p38 MAP kinase inhibitors for the treatment of inflammatory diseases: novel structures and developments during 2006−2008. *Curr. Top. Med. Chem.* **2008**, *8*, 1452–1467.

(10) Goldstein, D. G.; Kuglstatter, A.; Lou, Y.; Soth, M. J. Selective p38*a* inhibitors clinically evaluated for the treatment of chronic inflammatory disorders. *J. Med. Chem.* **2010**, *53*, 2345–2353.

(11) Hammaker, D.; Firestein, G. S. "Go upstream, young man": lessons learned from the p38 saga. *Ann. Rheum. Dis.* **2010**, *69*, i77–i82.

(12) Trejo, A.; Arzeno, H.; Browner, M. F.; Chanda, S.; Cheng, S.; Comer, D. D.; Dalrymple, S. A.; Dunten, P.; La Fargue, J.; Lovejoy, B.; Freire-Moar, J.; Lim, J.; McIntosh, J.; Miller, J.; Papp, E.; Reuter, D.; Roberts, R.; Sanpablo, F.; Saunders, J.; Song, K.; Villasenor, A.; Warren, S. D.; Welch, M.; Weller, P.; Whiteley, P, E.; Zeng, L.; Goldstein, D. M. Design and synthesis of 4-azaindoles as inhibitors of p38 MAP kinase. *J. Med. Chem.* **2003**, *46*, 4702–4713.

(13) Goldstein, D. M.; Alfredson, T.; Browner, M. F.; Dalrymple, S. A.; Dunn, J.; Freire-Moar, J.; Harris, S.; Labadie, S. S.; La Fargue, J.; Lapierre, J. M.; Li, F.; McWeeney, D.; Papp, E.; Ramesha, C.; Roberts, R.; Rotstein, D.; Sanpablo, B. F.; So, O.-Y.; Talamas, F. X.; Tao, W.; Trejo, A.; Villasenor, A.; Welch, T.; Weller, P.; Whiteley, P.; Young, K.; Zipfel, S. Discovery of *S*-[5-amino-1-(4-fluorophenyl)-1*H*-pyrazol-4-yl]-[3-(2,3-dihydroxypropoxy)phenyl]methanone (RO3201195), an orally bioavailable and highly selective inhibitor of p38 map kinase. *J. Med. Chem.* **2006**, *49*, 1562–1575.

(14) Harris, W.; Hill, C. H.; Smith, I. E. D. Preparation of Pyrimidopyrimidinones as T-Cell Tyrosine Kinase Inhibitors. PCT Int. Appl. WO 2000024744 A1, 2000.

(15) Chen, J. J.; Dunn, J. P.; Goldstein, D. M.; Stahl, C. M. Preparation of 2,6-disubstituted 7-oxopyrido[2,3-*d*]pyrimidines for treating p38 mediated disorders. WO2002064594, 2002.

(16) Hill, R. J.; Dabbagh, K.; Phippard, D.; Li, C.; Suttmann, R. T.; Welch, M.; Papp, E.; Song, K. W.; Chang, K.-c.; Leaffer, D.; Kim, Y.-N.; Roberts, R. T.; Zabka, T. S.; Aud, D.; Dal Porto, J.; Manning, A. M.; Peng, S. L.; Goldstein, D. M.; Wong, B. R. Pamapimod, a novel p38 mitogen-activated protein kinase inhibitor: preclinical analysis of efficacy and selectivity. *J. Pharmacol. Exp. Ther.* **2008**, *327* (3), 610–619.

(17) Alten, R. E.; Zerbini, C.; Jeka, S.; Irazoque, F.; Khatib, F.; Emery, P.; Bertasso, A.; Rabbia, M.; Caulfield, J. P. Efficacy and safety of pamapimod in patients with active rheumatoid arthritis receiving stable methotrexate therapy. *Ann. Rheum. Dis.* **2010**, *69*, 364–367.

(18) Cohen, S. B.; Cheng, T. T.; Chindalore, V.; Damjanov, N.; Burgos-Vargas, R.; Delora, P.; Zimany, K.; Travers, H.; Caulfield, J. P. Evaluation of the efficacy and safety of pamapimod, a p38 MAP kinase inhibitor, in a double-blind, methotrexate-controlled study of patients with active rheumatoid arthritis. *Arthritis Rheum.* **2009**, *60*, 335–344.

(19) Genovese, M. C. Inhibition of p38: Has the fat lady sung? *Arthritis Rheum.* **2009**, *60*, 317–320.

(20) Dunn, J. P.; Fisher, L. E.; Goldstein, D. M.; Harris, W.; Hill, C. H.; Smith, I. E. D.; Welch, T. R. Preparation of Alkylamino Substituted Bicyclic Nitrogen Heterocycles for Pharmaceutical Use as Inhibitors of p38 Protein Kinase. PCT Int. Appl. WO 2001029042 A1, 2001.

(21) Paulini, R.; Müller, K.; Diederich, F. Orthogonal multipolar interactions in structural chemistry and biology. *Angew. Chem., Int. Ed.* **2005**, *44*, 1788–1805.

(22) Müller, K.; Faeh, C.; Diederich, F. Fluorine in pharmaceuticals: looking beyond intuition. *Science* **2007**, *317*, 1881–1886.

(23) Fabian, M. A. B.; William, H.; Treiber, D. K.; Atteridge, C. E.; Azimioara, M. D.; Benedetti, M. G.; Carter, T. A.; Ciceri, P.; Edeen, P. T.; Floyd, M.; Ford, J. M.; Galvin, M.; Gerlach, J. L.; Grotzfeld, R. M.; Herrgard, S.; Insko, D. E.; Insko, M. A.; Lai, A. G.; Lelias, J.; Mehta, S. A.; Milanov, Z. V.; Velasco, A. M.; Wodicka, L. M.; Patel, H. K.; Zarrinkar, P. P.; Lockhart, D. J. A small molecule−kinase interaction map for clinical kinase inhibitors. *Nat. Biotechnol.* **2005**, *23*, 329–336.